Electron-impact excitation of Fe^{21+}, including $n = 4$ levels

N R Badnell[1], D C Griffin[2] and D M Mitnik[2]

[1] Department of Physics and Applied Physics, University of Strathclyde, Glasgow G4 0NG, UK
[2] Department of Physics, Rollins College, Winter Park, FL 32789, USA

Abstract
We have carried out a 204-level close-coupling (CC) calculation for B-like
Fe using the *R*-matrix method in conjunction with the intermediate-coupling
frame transformation method as part of the RmaX Network programme of
work to provide atomic data for x-ray processes. We have also carried out
two 125-level CC calculations to enable us to illustrate the effect of $n = 4$
levels on collision data involving $n = 2$ and 3 levels and to provide a
quantitative guide to the uncertainty resulting from the partial resolution of
resonances. From our 204-level CC calculation, we have generated effective
collision strengths over $T = 10^5$–10^8 K for all 20 706 inelastic transitions,
which is an order of magnitude larger than has been generated hitherto. We
provide illustrative comparisons with the results of previous workers, where
possible, and find a broad accord. The consistent and comprehensive set
of data that we have generated (energy levels, radiative rates and effective
collision strengths, including Born limits) is of great relevance to studies
utilizing spectral observations from the new high-resolution x-ray satellites
Chandra and *XMM–Newton*, as well as being necessary for the collisional–
radiative modelling of metallic impurities that will arise in the next generation
of magnetic fusion reactors.

1. Introduction

The interpretation of spectral emission observations made with the new high-resolution x-
ray satellites *Chandra* and *XMM–Newton* requires collision data for iron ions beyond the
scope of those readily available, for example from the IRON Project (Hummer *et al* 1993).
Similarly, the collisional–radiative modelling of metals for the next generation of magnetic
fusion devices requires extensive collision data. Consequently, the RmaX Network[3] was
formed to study both inner-shell electron and photon-induced collisions, as well as extensive
outer-shell excitations of ions of elements of interest to fusion and astrophysics, especially

[3] Available at http://amdpp.phys.strath.ac.uk/UK_RmaX/

photoionized plasmas, all using the R-matrix method. In contrast to the Breit–Pauli (BP) R-matrix approach (Scott and Burke 1980) of the IRON Project, extensive use is being made of the LS-coupling R-matrix method (including the mass–velocity and Darwin operators) in conjunction with the intermediate-coupling frame transformation (ICFT) method (Griffin *et al* 1998) to take account of spin–orbit effects. Such an approach is much less computationally demanding than the equivalent-sized full BP approach, while being just as accurate, for all practical purposes (Griffin and Badnell 2000). This enables data to be computed more rapidly or larger-scale calculations to be attempted.

In the case of Fe ions, H-like (Ballance *et al* 2001b) and He-like (Whiteford *et al* 2001) effective collision strengths have been computed for all levels up to the $n = 5$ shell, allowing for the effect of radiation damping of resonances. Inner-shell electron (photon) collisions with Li-like (Be-like) Fe have been studied by Ballance *et al* (2001a), with work in progress on the Be-like (B-like) system. Outer-shell electron-impact excitation of C-like Fe, including $n = 4$ levels, has been studied by Badnell and Griffin (2001) via a 200-level close-coupling (CC) ICFT calculation, and effective collision strengths provided for all 19 900 inelastic transitions over $T \approx 10^5$–10^8 K. Similar-scale calculations are in progress on N-like (McLaughlin, private communication) and O-like (Butler, private communication) Fe. In this paper we report on a 204CC calculation for B-like Fe^{21+} along the lines of our work on Fe^{20+} (Badnell and Griffin 2001). Here though, by performing two 125CC ICFT calculations, we look more closely at the problem of resonance resolution in highly charged ions and the effect of including $n = 4$ CC levels, and the resonances attached to them, on transitions within and between $n = 2$ and 3 levels.

Relativistic distorted-wave collision strengths for B-like Fe have been calculated by Zhang and Sampson (1994a, 1994b) for all transitions both within the $n = 2$ complex and to $n = 3$. The most comprehensive and reliable R-matrix results to date for Fe^{21+}, especially for application purposes, are those of Zhang and Pradhan (1997). They carried out a 45CC-level BP R-matrix calculation and provided effective collision strengths for all 990 inelastic transitions. Essentially, they allowed for $2p \rightarrow 3l$ and $2s \rightarrow 3s$, 3p promotions out of the $2s^2 2p$ ground configuration, as well as including all levels from the $n = 2$ complex of course. In this work, in addition, we allow for all $2s \rightarrow 3d$, $2s \rightarrow 4l$ and $2p \rightarrow 4l$ promotions out of the ground configuration and $2s \rightarrow 3l$ promotions out of the $2s2p^2$ first excited configuration (2p promotions from here are already included as 2s promotions from the ground configuration). This leads us to a 204CC–level ICFT R-matrix calculation, from which we provide effective collision strengths for all 20 706 inelastic transitions.

The structure of this paper is as follows: in section 2 we briefly review the theory behind our work. In section 3, we discuss the details of our calculations for Fe^{21+} and, in particular, the issue of resonance resolution. In section 4, we present illustrative results for both ordinary and effective collision strengths and comment on the comparison with the results of Zhang and Pradhan (1997) and of Zhang and Sampson (1994b). We finish with a short conclusion.

2. Theory

We follow closely the approach that we used for Fe^{20+} (Badnell and Griffin 2001). Our basic approach to the solution of the collision problem is to use the R-matrix method (Burke and Berrington 1993) in conjunction with the ICFT method (Griffin *et al* 1998). A complete solution, in terms of reactance or scattering (collision) matrices, is obtained first in LS-coupling. In particular, use is made of multi-channel quantum defect theory (MQDT) to obtain 'unphysical' collision matrices (Gorczyca and Badnell 2000). These are then transformed, first, algebraically to jK-coupling and then, via the use of term-coupling
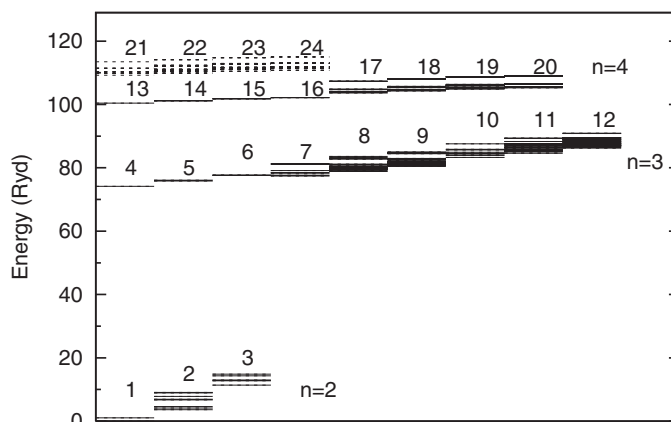
Figure 1. Energy level representation for Fe^{21+}. The solid lines denote the 204CC levels and the broken lines the purely CI levels. The upper bounding box delineates the ionization limit. The indices refer to the configuration numbers given in table 1.

Table 1. Configurations included for Fe^{21+}.

1	$2s^2 2p$	2	$2s2p^2$	3	$2p^3$		
4	$2s^2 3s$	5	$2s^2 3p$	6	$2s^2 3d$		
7	$2s2p3s$	8	$2s2p3p$	9	$2s2p3d$		
10	$2p^2 3s$	11	$2p^2 3p$	12	$2p^2 3d$		
13	$2s^2 4s$	14	$2s^2 4p$	15	$2s^2 4d$	16	$2s^2 4f$
17	$2s2p4s$	18	$2s2p4p$	19	$2s2p4d$	20	$2s2p4f$
21	$2p^2 4s$	22	$2p^2 4p$	23	$2p^2 4d$	24	$2p^2 4f$

coefficients, to intermediate coupling. Such an approach is typically an order of magnitude less demanding of computer resources than the equivalent full BP R-matrix calculation. Furthermore, the transformation of the 'unphysical' collision matrices ensures that accurate results are obtained in the resonance region. See Badnell and Griffin (2001) for further discussion of our approach.

3. Application to Fe^{21+}

3.1. Structure

In table 1 we list the 24 configurations that make up our configuration interaction (CI) expansion. These give rise to 130 terms and 291 levels. The 204 levels included in our largest CC expansion are all of those that arise from configurations 1–20 while our 125-level CC calculation used those from configurations 1–12. In both cases, all purely CI levels lie above the highest CC level. The 45CC levels of Zhang and Pradhan (1997) correspond to all of those that arise from configurations 1–8, but they do not correspond to the 45 levels lowest lying in energy in Fe^{21+}—see figure 1.

We used AUTOSTRUCTURE (Badnell 1986, 1997) to generate our atomic structure and, hence, the radial orbitals for the R-matrix calculation. We used the same nl-dependent scaling

Table 2. Some energy levels (Ryd) of Fe^{21+}.

Index	Configuration	Level	Observed[a]	AS[b]	SS[c]
1	$2s^2 2p$	$^2P_{1/2}$	0.0	0.0	0.0
2	$2s^2 2p$	$^2P_{3/2}$	1.0778	1.0615	1.0563
3	$2s2p^2$	$^4P_{1/2}$	3.6865	3.6186	3.6344
4	$2s2p^2$	$^4P_{3/2}$	4.1937	4.1172	4.1308
5	$2s2p^2$	$^4P_{5/2}$	4.6772	4.6285	4.6406
6	$2s2p^2$	$^2D_{3/2}$	6.7117	6.7166	6.7386
7	$2s2p^2$	$^2D_{5/2}$	6.9222	6.9256	6.9450
8	$2s2p^2$	$^2P_{1/2}$	7.7775	7.7979	7.8227
9	$2s2p^2$	$^2S_{1/2}$	8.9142	8.9204	8.9349
10	$2s2p^2$	$^2P_{3/2}$	9.0424	9.0673	9.0988
11	$2p^3$	$^4S_{3/2}$	11.443	11.391	11.435
12	$2p^3$	$^2D_{3/2}$	12.725	12.720	12.771
13	$2p^3$	$^2D_{5/2}$	13.003	13.024	13.075
14	$2p^3$	$^2P_{1/2}$	14.304	14.325	14.371
15	$2p^3$	$^2P_{3/2}$	14.833	14.854	14.886

[a] Sugar and Corliss (1985).
[b] AUTOSTRUCTURE (this paper).
[c] SUPERSTRUCTURE (Zhang and Pradhan 1997).

parameters for the Thomas–Fermi–Dirac–Amaldi statistical potential as we did for Fe^{20+} (Badnell and Griffin 2001).

In table 2 we compare the energies of our lowest 15 levels with those resulting from the 45-level calculation with SUPERSTRUCTURE by Zhang and Pradhan (1997), as well as with observed values (Sugar and Corliss 1985). We see that the differences between the two sets of theoretical results are smaller than are those with the observed, in general.

3.2. Collision

We carried out LS-coupling inner-region R-matrix calculations, including the mass–velocity and Darwin operators, using codes that were originally based on the published exchange (Berrington *et al* 1995) and non-exchange (Burke *et al* 1992) R-matrix codes. In the case of the 204CC-level calculation, we used a 97CC-term expansion consisting of the 92 terms necessary to generate the pure 204CC-level expansion discussed above, plus an additional five terms that gave rise to components in the term-coupling coefficient expansion for the 204CC levels that were larger than 0.01. In the case of the 125CC-level calculation, we only needed to use the 58CC-term expansion necessary to generate the pure 125CC-level expansion. In addition, since our LS-coupling CC expansion is smaller than our CI expansion, we necessarily constructed a balanced 'correlation' expansion following Gorczyca *et al* (1995).

The outer-region solutions were obtained using our MQDT version of Seaton's unpublished STGF code; this treats all closed channels as 'open' (Gorczyca and Badnell 2000). The ICFT calculation was made with our unpublished STGICF and STGICFDAMP codes for working with the unphysical reactance and scattering matrices, respectively. (Working with the latter became significantly more efficient when about two-thirds of the target levels were open.) The entire suite of codes is supported by the UK RmaX Network and it is available from its website under http://amdpp.phys.strath.ac.uk/UK_RmaX/codes.html .

3.2.1. High angular momentum. We carried out our exchange calculations up to $J = 11$ and our non-exchange calculations from there on up to $J = 38$. The 'top-up' contribution (from higher J) for dipole transitions was computed using the Burgess (1974) sum rule. In addition, the top-up contribution for non-dipole transitions was computed assuming a geometric series in energy and taking care to switch over smoothly to the degenerate-energy limiting case (Burgess *et al* 1970). We compared the summed collision strength with top-up to that without top-up at every energy and for every transition. About 50 non-dipole transitions had a top-up contribution that was greater than 30% of the total, with the largest being about 50%. In the dipole case, the contribution from top-up becomes increasingly large for near-degenerate transitions[4]. The top-up becomes infinite in the formal case of exact degeneracy because the total collision strength diverges logarithmically. The only requirement for the use of the Burgess (1974) sum rule is that the Coulomb Bethe approximation be valid. This becomes increasingly accurate for near-degenerate transitions as the total collision strength is dominated by contributions from increasingly large angular momentum. The largest dipole top-up (a factor of ≈ 11) occurred for the $2s2p4p\,^4P_{3/2}$–$2s2p4d\,^2D_{3/2}$ transition. Examination of the reduced high-energy collision strength showed it to be tending correctly to its reduced infinite-energy limit-value. About 1700 dipole transitions had a top-up contribution that was greater than 50% of the total.

3.2.2. High-temperature limit. We used 24 basis orbitals to represent the continuum electron's wavefunction initially; this number was progressively reduced automatically in the non-exchange calculations as the scattering angular momentum increased. This enabled us to calculate total collision strengths explicitly up to 440 Ry. For allowed transitions, collision strengths were calculated at higher energies by interpolating the reduced collision strength, as a function of reduced scattering energy, between the values up to 440 Ry and the infinite-energy limit-point, following Burgess and Tully (1992). In our work on Fe^{20+} (Badnell and Griffin 2001) we only had this limit point available to us for dipole transitions. Here, we use the infinite-energy Born limit (Burgess *et al* 1997) for non-dipole-allowed transitions. Its computation has been implemented within AUTOSTRUCTURE (Badnell and Thomas, unpublished[5]) and it is discussed in more detail by Whiteford *et al* (2001). As a result, the remaining forbidden transition collision strengths were extrapolated as $E^{-\alpha}$, with $\alpha = 1$–2. We tabulate effective collision strengths up to 10^8 K, at which temperature the coronal fractional abundance of Fe^{21+} is about 10^{-5} (Arnaud and Raymond 1992).

3.2.3. Weakly allowed transitions. Virtually every transition is at least weakly allowed in a large ICFT calculation. Only 53 transitions out of 20 706 do not have an infinite-energy Born or dipole limit-value in our 204CC calculation. Transitions that involve a two-, or more-, electron jump in the target only take place through electrostatic mixing. If this mixing is uncertain then this leads to large uncertainties in the resulting ordinary and effective collision strengths. Another class of weakly allowed transitions are those that can only take place through electron exchange in LS-coupling. They can become weakly Born or dipole allowed through spin–orbit mixing. At high energy (temperature) this Born or dipole characteristic completely dominates the ordinary (effective) collision strength. So, again, any uncertainty in the mixing will lead directly to uncertainty in the collision strength.

---

[4] In our work on Fe^{20+} (Badnell and Griffin 2001) we stated that the dipole top-up was at most a few per cent. In fact, it is similar to that found here. We originally compared our dipole topped-up results with those that contained a different dipole top-up, not one that omitted it.

[5] The program AUTOSTRUCTURE is available from http://amdpp.phys.strath.ac.uk/autos/

3.2.4. Low-temperature limit. The low-temperature limit of our effective collision strength tabulation follows from the fact that the vast majority of the energy levels have not been observed. Low-temperature effective collision strengths are sensitive to the presence and/or absence of resonances just above each threshold, along with their resolution. We investigated this problem in detail in our study on Fe^{20+} (Badnell and Griffin 2001). Based on that study, and given the uncertainty in the value of the calculated $n > 2$ level energies, our lowest recommended temperature for transitions involving these levels is $\log_{10}(T(K)) = 6.4$. Errors of $\sim 30\%$ are still possible at this temperature, but these rapidly diminish with increasing temperature. While the coronal fractional abundance is small ($< 10^{-5}$) here, this may not be the case for a photoionized plasma. However, at lower electron temperatures it is transitions between low-lying (e.g. $n = 2$) levels that are the most important. Since we have used the observed $n = 2$ level energies in our 204CC calculations for Fe^{21+}, our 204CC effective collision strengths amongst the $n = 2$ levels can be extended to lower temperatures; we tabulate them down to 10^5 K.

3.3. Resonance resolution.

Resolution of the resonance structure becomes increasingly laborious as the residual charge-state (z) of an ion increases because the number of energy points should increase as z^2 so as to maintain the same level of resolution. We chose to use the same z-scaled energy mesh as we did for Fe^{20+}, namely, a step of $1 \times 10^{-5} z^2$ Ry through energy regions where $\delta n = 0$ resonances were present, a step of $4 \times 10^{-5} z^2$ Ry where only $\delta n = 1$ resonances were present and, finally, a step of $0.01 z^2$ Ry above all thresholds. This resulted in a total of 13 327 energies being used. Although this energy mesh is sufficient to resolve the dominant resonance structure, a large number of weaker resonances are only partially resolved. A step of $\sim 10^{-9} z^2$ Ry for $\delta n = 0$ resonances and a step of $\sim 10^{-7} z^2$ Ry for $\delta n = 1$ resonances would be required before narrower resonances could be assumed to be significantly radiation damped. Zhang and Pradhan (1997) allowed for the effect of radiation damping. Even by resolving resonances attached to $n = 2$ thresholds up to an effective quantum number of 45, they found little effect on the effective collision strengths. We have a larger energy range to span. The mesh that we have detailed above is orders of magnitude coarser than the dominant radiative widths and so in the first place almost completely omits the contribution from resonances that would be damped away.

We argued previously (Badnell and Griffin 2001) for the retention of partially resolved resonances on statistical grounds, there being a large degree of cancellation between over- and under-estimates. We use the same approach here for the determination of effective collision strengths from our 204CC calculation. We examined the value of the collision strength for every transition (20 706 of them) at every energy in the resonance region ($\approx 13\,000$ of them) and found 320 data points for which the collision strength differed by a factor of 1000 or more from the value of the point at either side, while $\approx 10\,500$ of them differed by a factor of 100 or more. This is to be compared with the total number of data points ~ 100 million. Given that the 320 data points represent the most extreme range of the statistics and the ones most likely to be subject to any numerical failure, we chose to eliminate (only) those points. The only effective collision strengths significantly affected (by more than a factor of 1.5) by this procedure were those for about 20 transitions which were between levels which differ by two electrons.

In order to investigate the statistical approach quantitatively, we carried out two 125CC calculations using two different energy meshes. The first one was that detailed above and the second one was that resulting from using four times as many points in each energy region. In each case, no resonances were eliminated. Firstly, for the 105 transitions between the 15 $n = 2$ levels, we observed no differences exceeding 30% between the two sets of resulting effective

collision strengths at temperatures above 10^6 K. At 10^5 K, differences ranged between 30% and 70% for nine transitions; this difference falls off rapidly with increasing temperature.

Extending the comparison to include the 7645 transitions involving $n = 3$ levels as well, we found differences exceeding 30% between the two sets of results for 199 transitions at temperatures above $\log_{10}(T(\text{K})) = 6.4$; the difference just exceeded a factor of two for five transitions. Scanning through these 199 transitions we find that the vast majority of them involve two-electron jumps.

Finally, we note that eliminating points from our coarse-mesh collision strength file that were a factor of five or ten larger than adjacent points both resulted in substantially worse agreement with the results obtained using the finer energy mesh.

4. Results

Our 204CC-level calculation gives rise to a large amount of data, e.g. effective collision strengths for 20 706 transitions, and so we only present some illustrative results for comparison here. The full set of results for energy levels, dipole radiative rates and effective collision strengths (including Born limits), tabulated in the ADAS *adf04* format (Summers 1994, 1999), is available via the WWW under http://www-cfadc.phy.ornl.gov/data_and_codes/. The effective collision strengths (Seaton 1953) are tabulated over[6] $T = 10^5$–10^8 K, which comfortably exceeds the temperature of peak coronal fractional abundance ($\sim 10^7$ K) for Fe^{21+} and spans the lower temperatures of interest for studies on photoionized plasmas.

We emphasize that the only difference between our 125CC and 204CC calculations is the inclusion of $n = 4$ CC levels in the latter. Everything else remains unchanged, for example CI, energy mesh, top-up etc. Thus, the differences that we observe between these two sets of results are due solely to the $n = 4$ CC levels. In the case of the comparisons with the 45CC results of Zhang and Pradhan (1997), the differences in the CI, energy mesh etc used may also contribute to any differences noted between the respective effective collision strengths.

4.1. $n = 2$ to $n' = 2$

In table 3 we compare effective collision strengths for transitions from the ground level to the 14 excited $n = 2$ levels, at two temperatures. The lower temperature corresponds to that where resonances attached to $n = 2$ levels can be expected to dominate any resonant enhancement while the higher one corresponds to that where resonances attached to $n > 2$ levels can be important.

The first thing to note is that, at the lower temperature especially, the effective collision strengths can be sensitive to the position of the target levels. A comparison of our two sets of 204CC results, obtained using observed and calculated $n = 2$ target level energies, demonstrates this. As noted previously, results for these transitions are not too sensitive to the two energy meshes that we used. Our 125CC results obtained using the fine energy mesh (not shown) differ little from the standard-mesh results. Transition 1–2 is an exception; the fine-mesh result (9.65×10^{-2}) is actually close to the 204CC value (9.86×10^{-2}). Zhang and Pradhan (1997) actually set their level energies within a term to be degenerate and equal to the value of the observed level-weighted average (Zhang, private communication). It is curious that our results obtained using our calculated level energies are in somewhat better agreement with those of Zhang and Pradhan (1997) than those we obtained using the observed level energies. In any case, the differences observed in the effective collision strengths at $\log_{10}(T(\text{K})) = 5.64$

---

[6] However, bear in mind the caveats given in section 3 and which are repeated in the *adf04* file.

Table 3. Effective collision strengths in Fe^{21+} from level 1 to all other levels of the $n = 2$ complex.

	$\log T_{10}(\mathrm{K}) = 5.64$				$\log T_{10}(\mathrm{K}) = 6.34$			
	ICFT				ICFT			
j^a	204CC[b]	204CC[c]	125CC[c]	45CC BP[d]	204CC[b]	204CC[c]	125CC[c]	45CC BP[d]
2	8.93(−2)[e]	9.86(−2)	8.39(−2)	1.51(−1)	6.96(−2)	7.50(−2)	7.14(−2)	8.89(−2)
3	1.67(−2)	1.45(−2)	1.45(−2)	1.23(−2)	1.28(−2)	1.23(−2)	1.24(−2)	1.18(−2)
4	1.33(−2)	1.43(−2)	1.38(−2)	1.31(−2)	9.55(−3)	9.95(−3)	9.89(−3)	9.00(−3)
5	1.06(−2)	1.40(−2)	1.48(−2)	1.29(−2)	8.48(−3)	9.65(−3)	9.85(−3)	7.99(−3)
6	2.45(−1)	2.48(−1)	2.45(−2)	1.97(−1)	2.66(−1)	2.67(−1)	2.67(−1)	2.52(−1)
7	7.55(−3)	1.08(−2)	8.27(−3)	1.09(−2)	8.38(−3)	9.11(−3)	8.52(−3)	6.31(−3)
8	2.64(−1)	2.65(−1)	2.64(−1)	2.44(−1)	2.84(−1)	2.84(−1)	2.84(−1)	2.92(−1)
9	9.82(−3)	9.81(−3)	9.80(−3)	1.10(−2)	1.18(−2)	1.18(−2)	1.19(−2)	1.33(−2)
10	5.50(−2)	5.50(−2)	5.48(−2)	5.20(−2)	6.03(−2)	6.03(−2)	6.04(−2)	5.99(−2)
11	3.75(−4)	3.45(−4)	3.64(−4)	3.34(−4)	4.63(−4)	4.57(−4)	4.67(−4)	4.38(−4)
12	1.06(−3)	1.04(−3)	1.07(−3)	9.89(−4)	1.31(−3)	1.30(−3)	1.28(−3)	1.19(−3)
13	6.28(−4)	5.97(−4)	5.96(−4)	5.70(−4)	8.97(−4)	8.90(−4)	8.77(−4)	7.38(−4)
14	7.98(−4)	8.02(−4)	7.86(−4)	7.71(−4)	1.11(−3)	1.11(−3)	1.07(−3)	9.36(−4)
15	1.33(−4)	1.33(−4)	1.25(−4)	1.13(−4)	5.75(−4)	5.74(−4)	5.03(−4)	2.80(−4)

[a] Upper-level index, see table 2.
[b] This paper, obtained using observed energy levels.
[c] This paper, obtained using calculated energy levels.
[d] Zhang and Pradhan (1997).
[e] $a(-b)$ denotes $a \times 10^{-b}$.

are understandable, given the sensitivity to the position of the $n = 2$ target levels. Zhang and Pradhan (1997, figure 1) have demonstrated that the relativistic distorted-wave results of Zhang and Sampson (1994a) can lead to significant underestimates of these effective collision strengths due to the omission of resonances, and we shall not repeat it.

At the higher temperature, given by $\log_{10}(T(\mathrm{K})) = 6.34$, there is evidence of enhancement of the weaker effective collision strengths due to the additional $n = 3$ levels that we include over the 45CC calculation of Zhang and Pradhan (1997). The results for transitions 1–7 and 1–15 also show an additional (small) enhancement due to the inclusion of $n = 4$ CC levels.

Zhang and Pradhan (1997) noted large differences, up to a factor of two, between their BP effective collision strengths and those that they obtained by term coupling the 'physical' collision matrices, e.g. for transitions 1–3, 4, 5, 9, 11, 14 (see their table 2). As expected, these differences are completely eliminated by our approach of term coupling the 'unphysical' collision matrices.

4.2. $n = 2$ to $n' = 3$

In figure 2(*a*) we show the 204CC collision strength for the transition[7] 1–16: $2s^2 2p\,{}^2P_{1/2}$–$2s^2 3s\,{}^2S_{1/2}$. The dominant resonance structure lies below 10 Ry (scattered energy), or 85 Ry relative to the initial ground level. These resonances are attached to levels included in the 45CC calculation of Zhang and Pradhan (1997). Consequently, we observe little difference between our 204CC and the 45CC results for the resulting effective collision strength, shown in figure 2(*b*). Our 125CC results start to rise a little above these two sets of results at the lowest temperatures, indicating the sensitivity to resonance resolution still. The $n = 4$ CC levels can affect the position of resonances attached to $n = 3$ levels in the 204CC calculation,

[7] The level indices are those tabulated in the *adf04* file.
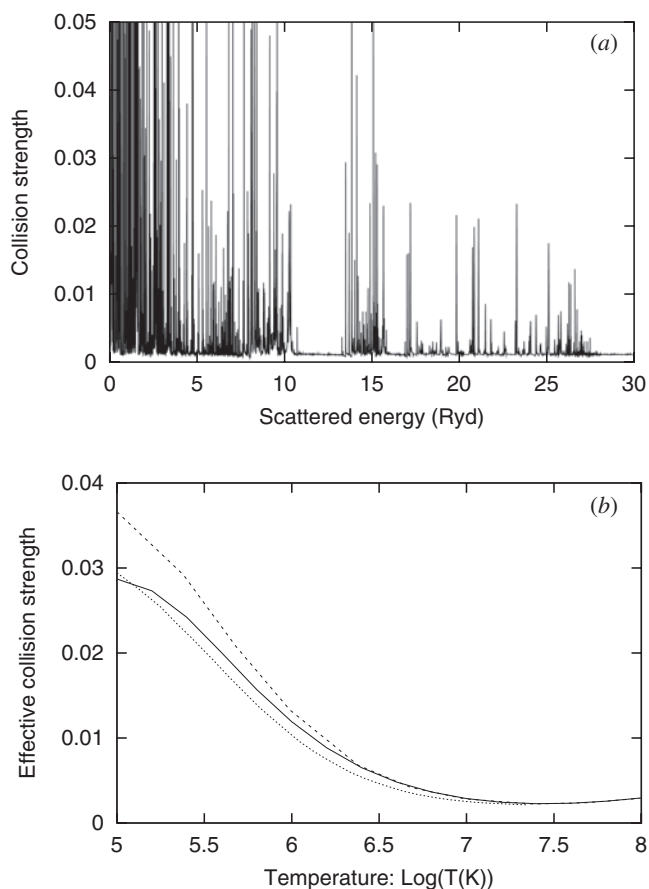
Figure 2. Transition 1–16: $2s^2 2p\ ^2P_{1/2}$–$2s^2 3s\ ^2S_{1/2}$ in Fe^{21+}. (*a*) Collision strength versus energy relative to the upper level (204CC, this paper). (*b*) Effective collision strengths: solid curve, 204CC ICFT (this paper); dashed curve, 125CC ICFT (this paper); dotted curve, 45CC BP (Zhang and Pradhan 1997).

via (N + 1)-electron CI mixing for example, compared with the 125CC calculation. Recall, section 3.2.4, that we recommend a low-temperature limit of $\approx 2.5 \times 10^6$ K for transitions involving $n > 2$ levels.

In figure 3(*a*) we show the 204CC collision strength for the transition 1–22: $2s^2 2p\ ^2P_{1/2}$–$2s^2 3d\ ^2D_{5/2}$. We now observe that the dominant resonance structure lies above 5 Ry (scattered energy), or 83 Ry relative to the initial ground level. These resonances are attached to levels that were not included in the 45CC calculation of Zhang and Pradhan (1997). Consequently, we observe a distinct difference between our 204CC and the 45CC results for the resulting effective collision strength, shown in figure 3(*b*). The lack of a distinct peak in our 125CC results at 10^6 K shows that the dominant resonances are attached to $n = 4$ levels.

In figure 4(*a*) we show the 204CC collision strength for the transition 1–36: $2s^2 2p\ ^2P_{1/2}$–$2s2p3p\ ^4P_{5/2}$. There are strong resonances present over a wide range of energies. The comparison of effective collision strengths in figure 4(*b*) demonstrates the strong enhancement due to resonances attached to levels of the 2s2p3d configuration (cf 125CC versus 45CC) and some additional enhancement due to resonances attached to $n = 4$ levels (cf 204CC versus 125CC).
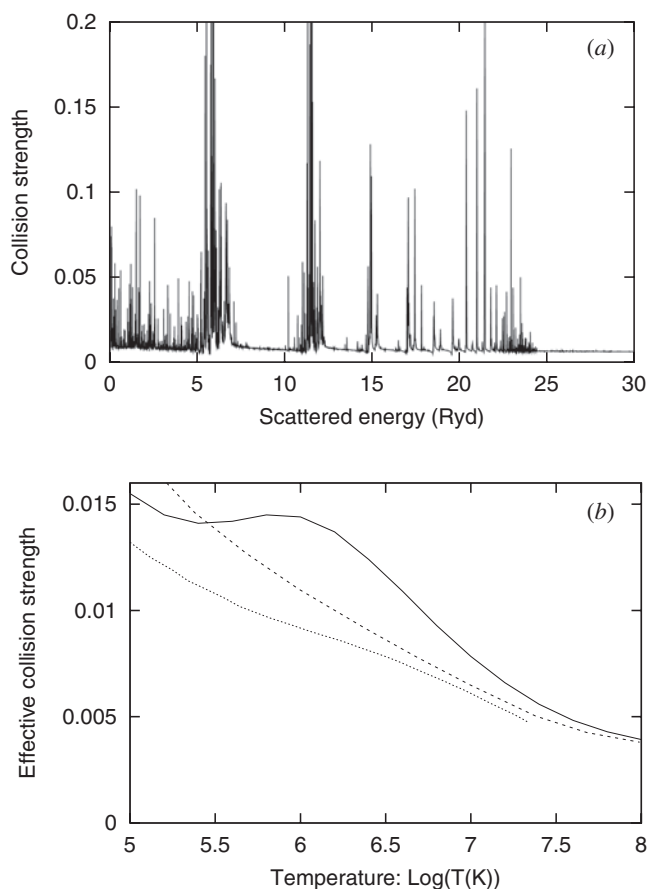
Figure 3. Transition 1–22: $2s^2 2p\ ^2P_{1/2}$–$2s^2 3d\ ^2D_{5/2}$ in Fe^{21+}. (*a*) Collision strength versus energy relative to the upper level (204CC, this paper). (*b*) Effective collision strengths: solid curve, 204CC ICFT (this paper); dashed curve, 125CC ICFT (this paper); dotted curve, 45CC BP (Zhang and Pradhan 1997).

In figure 5 we show the 204CC collision strength for (*a*) the transition 1–43: $2s^2 2p\ ^2P_{1/2}$–$2s2p3d\ ^4D_{1/2}$, and (*b*) the transition 1–45: $2s^2 2p\ ^2P_{1/2}$–$2s2p3s\ ^2P_{1/2}$. In both, we show the relativistic distorted-wave collision strengths of Zhang and Sampson (1994b) as well. We find the two upper levels to be highly mixed (almost 50%–50%). The difference between the 204CC and distorted-wave results may simply be due to different degrees of mixing. The sums of the background collision strengths to the two upper levels are quite similar. The resonance structure is not particularly strong. This is reflected in the 125CC and 204CC effective collision strengths shown in figure 5(*c*). However, the 45CC results of Zhang and Pradhan (1997) rise above our results at higher temperatures. They included only the upper level (our index 45) in their CC expansion.

4.3. $n = 4$ levels

There appear to be no prior published R-matrix or distorted-wave collision data involving the $n = 4$ levels. Our effective collision strengths for these levels incorporate little in the
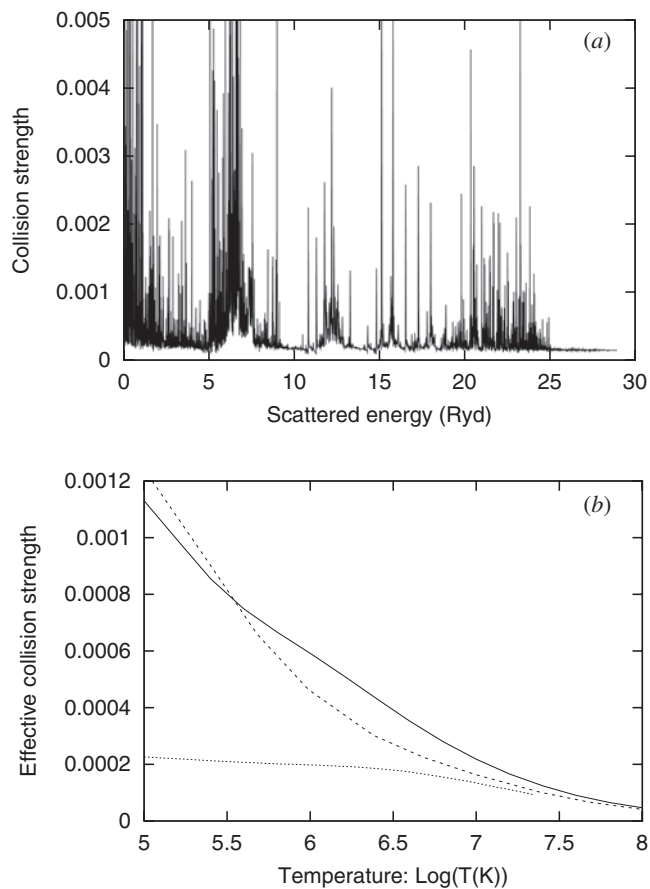
Figure 4. Transition 1–36: $2s^2 2p\ ^2P_{1/2}$–$2s2p3p\ ^4P_{5/2}$ in Fe^{21+}. (*a*) Collision strength versus energy relative to the upper level (204CC, this paper). (*b*) Effective collision strengths: solid curve, 204CC ICFT (this paper); dashed curve, 125CC ICFT (this paper); dotted curve, 45CC BP (Zhang and Pradhan 1997).

way of resonant enhancement. However, the main motivation for including these levels is to obtain a consistent and comprehensive set of data that could be used for modelling the soft-x-ray region. We can also compare our 125CC and 204CC results so as to assess the effect of coupling to $n = 4$ levels, especially resonances attached to them, on transitions to and between the $n = 2$ and 3 levels. In figures 6(*a*)–(*d*) we compare our effective collision strengths for the 7750 inelastic transitions that arise in the 125CC calculation, compared with the results from the 204CC calculation, over $T = 10^5$–10^8 K. We note the enhancement of the weaker effective collision strengths, which decreases with increasing temperatures. We also see a smaller reduction of some of the stronger effective collision strengths.

4.4. All transitions

In figure 7 we present effective collision strengths at 10^7 K for all 20 706 inelastic transitions from our 204CC calculation. In contrast to our results for Fe^{20+}, our omission of only the $2p^2 4l$ configurations from the 204-level CC expansion does not lead to such an obvious 'hole' in the
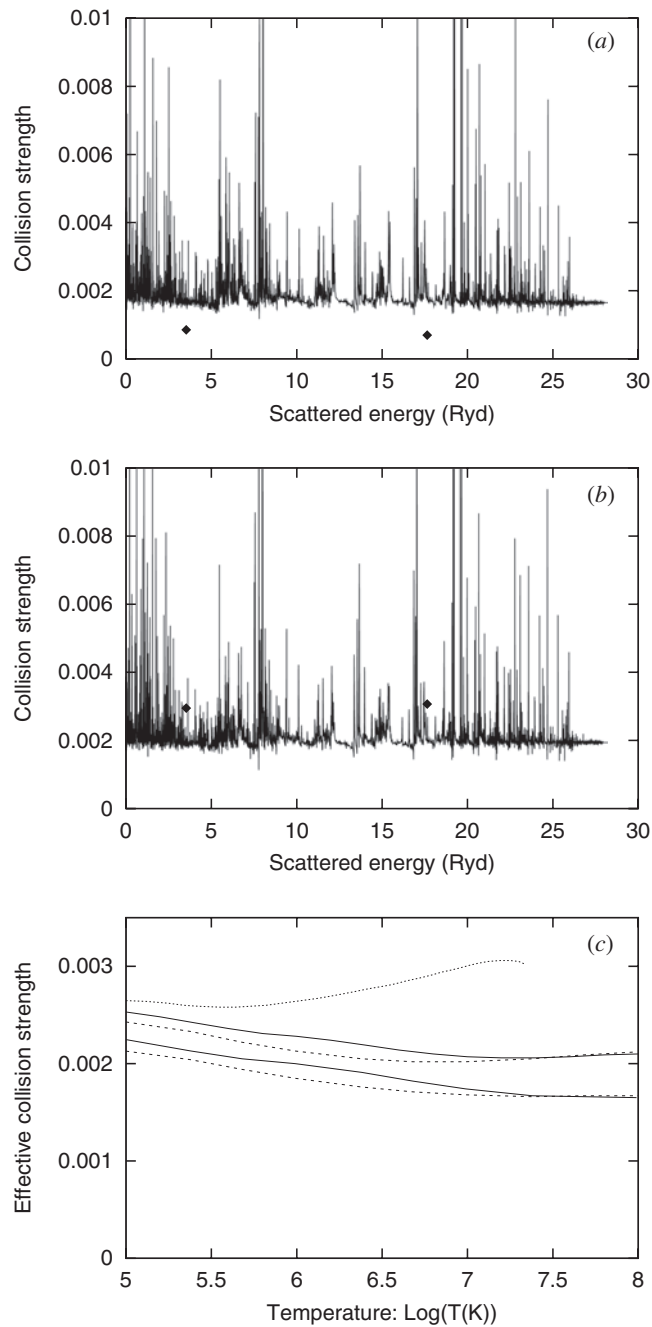
Figure 5. (*a*) Transition 1–43: $2s^22p$ $^2P_{1/2}$–$2s2p3d$ $^4D_{1/2}$ in Fe^{21+}. (*b*) Transition 1–45: $2s^22p$ $^2P_{1/2}$–$2s2p3s$ $^2P_{1/2}$ in Fe^{21+}. Collision strength versus energy relative to the upper level: solid curve, 204CC ICFT (this paper); diamonds, relativistic distorted wave (Zhang and Sampson 1994b). (*c*) Effective collision strengths: solid curve, 204CC ICFT (this paper); dashed curve, 125CC ICFT (this paper). The lower/upper ICFT pair is for transition 1–43/1–45. Dotted curve, 45CC BP (Zhang and Pradhan 1997) for transition 1–45.
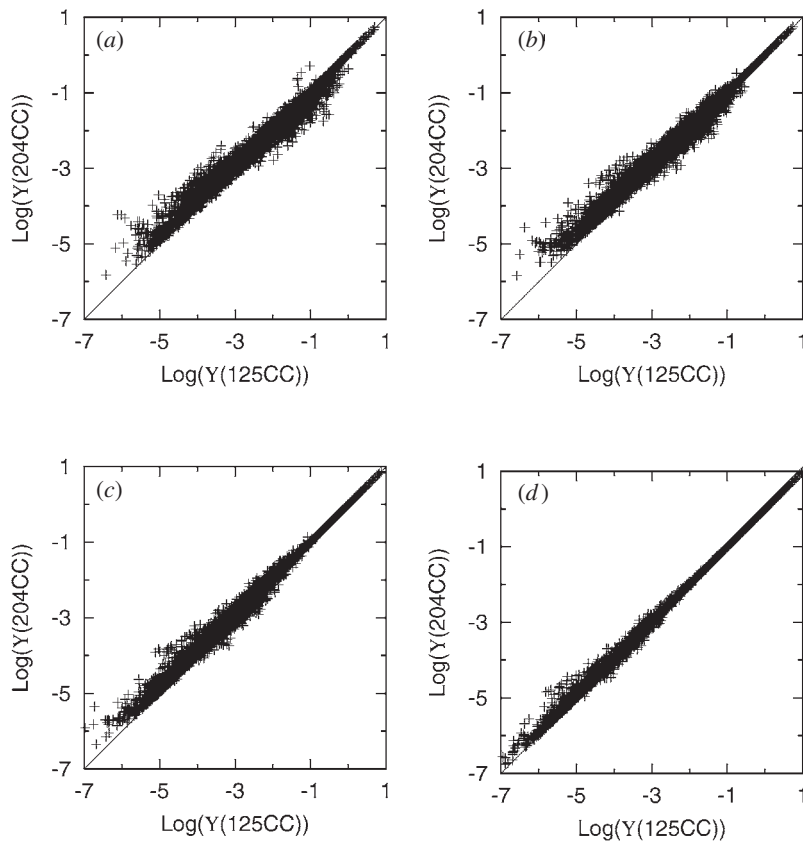
Figure 6. Effective collision strengths for the 7750 inelastic transitions that arise in the 125CC calculation, compared with the results from the 204CC calculation, at (a) 10^5 K, (b) 10^6 K, (c) 10^7 K and (d) 10^8 K. (All this paper.)

results for promotions from the $2p^3$ configuration (transitions 1986–2940). This is because of our inclusion of the $2p^23l$ configurations, which now allows for 2p to 3l promotions. However, the broad trend of the results from $n = 2$, 3 and 4 is the same as in the C-like case (Badnell and Griffin 2001). In particular, we note the stronger effective collision strengths for transitions between $n = 4$ levels.

5. Conclusion

We have carried out a 204-level CC calculation for Fe²¹⁺ using the R-matrix method in conjunction with the ICFT method as part of the RmaX Network programme of work to provide atomic data for x-ray processes. We have also carried out two 125CC-level calculations to enable us to illustrate the effect of $n = 4$ levels on collision data involving $n = 2$ and 3 levels, and to provide a quantitative guide to the uncertainty resulting from the partial resolution of resonances. From our 204CC calculation, we have generated effective collision strengths for all 20 706 inelastic transitions, which is an order of magnitude larger than has been generated hitherto. We find a broad accord with the (much smaller) set of data generated by Zhang and Pradhan (1997), using the BP R-matrix method, as part of the IRON Project. As expected,
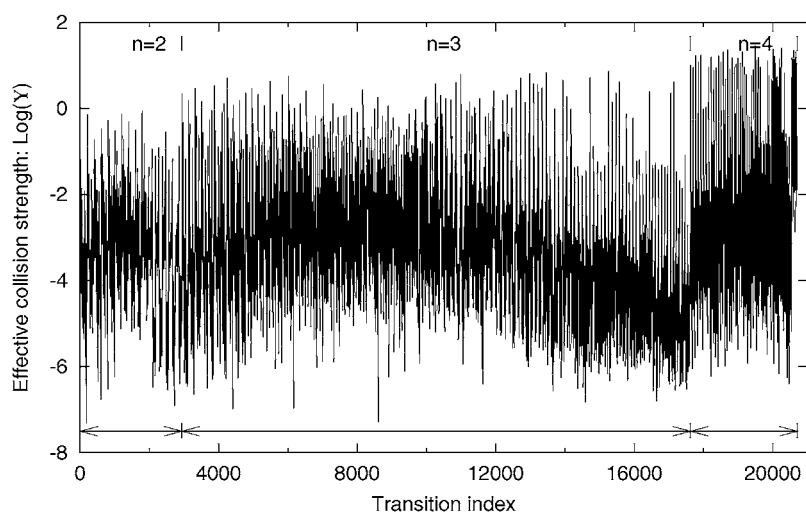
Figure 7. Effective collision strengths at a temperature of 10^7 K for 20 706 transitions in Fe^{21+}. The transition index (k) for the $i–j$ transition is given by $k : j = i + 1, 204, i = 1, 203$ where i denotes the lower level and j denotes the upper level. The label n in the figure denotes the principal quantum number of the initial level.

the main discrepancies arise on weak transitions where the additional resonance contributions that we provide for become paramount. The consistent and comprehensive set of data that we have generated (energy levels, radiative rates and effective collision strengths, including Born limits) is of great relevance to studies utilizing observations made by the new high-resolution x-ray satellites *Chandra* and *XMM–Newton*, as well as being necessary for the collisional–radiative modelling of metallic impurities that will arise in the next generation of magnetic fusion reactors.

Acknowledgments

References

Arnaud M and Raymond J 1992 *Astrophys. J.* **398** 394–406
Badnell N R 1986 *J. Phys. B: At. Mol. Phys.* **19** 3827–35
Badnell N R 1997 *J. Phys. B: At. Mol. Opt. Phys.* **30** 1–11
Badnell N R and Griffin D C 2001 *J. Phys. B: At. Mol. Opt. Phys.* **34** 681–97
Badnell N R and Tomas A L 2001 *Undergraduate Project Report* unpublished
Ballance C P, Badnell N R and Berrington K A 2001a *J. Phys. B: At. Mol. Opt. Phys.* **34** 3287–300
Ballance C P, Badnell N R and Berrington K A 2001b *J. Phys. B: At. Mol. Opt. Phys.* submitted

[8] The 204CC calculation was carried out completely on two SUN desktop workstations each containing a 333 MHz UltraSparc II processor. The STGICF/STGICFDAMP CPU memory requirement has been substantially reduced, down from 400 Mb (Badnell and Griffin 2001) to 200 Mb per processor.

Berrington K A, Eissner W B and Norrington P H 1995 *Comput. Phys. Commun.* **92** 290–420

Burgess A 1974 *J. Phys. B: At. Mol. Phys.* **7** L364–7

Burgess A, Chidichimo M C and Tully J A 1997 *J. Phys. B: At. Mol. Opt. Phys.* **30** 33–57

Burgess A, Hummer D G and Tully J A 1970 *Phil. Trans. R. Soc.* A **266** 225–79

Burgess A and Tully J A 1992 *Astron. Astrophys.* **254** 436–53

Burke P G and Berrington K A 1993 *Atomic and Molecular Processes—an R-Matrix Approach* (Bristol: Institute of Physics Publishing)

Burke V M, Burke P G and Scott N S 1992 *Comput. Phys. Commun.* **69** 76–98

Gorczyca T W and Badnell N R 2000 *J. Phys. B: At. Mol. Opt. Phys.* **33** 2511–23

Gorczyca T W, Robicheaux F, Pindzola M S, Griffin D C and Badnell N R 1995 *Phys. Rev.* A **52** 3877–88

Griffin D C and Badnell N R 2000 *J. Phys. B: At. Mol. Opt. Phys.* **33** 4389–408

Griffin D C, Badnell N R and Pindzola M S 1998 *J. Phys. B: At. Mol. Opt. Phys.* **31** 3713–27

Hummer D G, Berrington K A, Eissner W, Pradhan A K, Saraph H E and Tully J A 1993 *Astron. Astrophys.* **279** 298–309

Scott N S and Burke P G 1980 *J. Phys. B: At. Mol. Phys.* **13** 4299–314

Seaton M J 1953 *Proc. R. Soc.* A **218** 400–16

Sugar J and Corliss C 1985 *J. Phys. Chem. Ref. Data* **14** Suppl 2

Summers H P 1994 *JET Joint Undertaking Report* JET-IR(94)06

Summers H P 1999 *ADAS User Manual Version 2.1* webpage http://adas.phys.strath.ac.uk

Whiteford A D, Badnell N R, Ballance C P, O'Mullane M G, Summers H P and Thomas A L 2001 *J. Phys. B: At. Mol. Opt. Phys.* **34** 3179–91

Zhang H L and Pradhan A K 1997 *Astron. Astrophys. Suppl. Ser.* **123** 575–80

Zhang H L and Sampson D H 1994a *At. Data Nucl. Data Tables* **56** 41–104

Zhang H L and Sampson D H 1994b *At. Data Nucl. Data Tables* **58** 255–305